Geophysical Journal International

Geophys. J. Int. (2011) **187,** 214–224 doi: 10.1111/j.1365-246X.2011.05131.x

A distribution-based parametrization for improved tomographic imaging of solute plumes

Adam Pidlisecky,[1] Kamini Singha[2] and Frederick D. Day-Lewis[3]

[1] *Department of Geosciences, University of Calgary,* 2500 *University Drive Northwest, Calgary,* AB T2N1N4*, Canada. E-mail: adampid@ucalgary.ca*
[2] *Department of Geosciences, The Pennsylvania State University, 311 Deike Building, University Park,* PA 16802*, USA*
[3] *U.S. Geological Survey, Office of Groundwater, Branch of Geophysics, 11 Sherman Place, Unit 5015, Storrs,* CT 06269*, USA*

Accepted 2011 June 28. Received 2011 February 17; in original form 2010 July 13

SUMMARY

Difference geophysical tomography (e.g. radar, resistivity and seismic) is used increasingly for imaging fluid flow and mass transport associated with natural and engineered hydrologic phenomena, including tracer experiments, *in situ* remediation and aquifer storage and recovery. Tomographic data are collected over time, inverted and differenced against a background image to produce 'snapshots' revealing changes to the system; these snapshots readily provide qualitative information on the location and morphology of plumes of injected tracer, remedial amendment or stored water. In principle, geometric moments (i.e. total mass, centres of mass, spread, etc.) calculated from difference tomograms can provide further quantitative insight into the rates of advection, dispersion and mass transfer; however, recent work has shown that moments calculated from tomograms are commonly biased, as they are strongly affected by the subjective choice of regularization criteria. Conventional approaches to regularization (Tikhonov) and parametrization (image pixels) result in tomograms which are subject to artefacts such as smearing or pixel estimates taking on the sign opposite to that expected for the plume under study. Here, we demonstrate a novel parametrization for imaging plumes associated with hydrologic phenomena. Capitalizing on the mathematical analogy between moment-based descriptors of plumes and the moment-based parameters of probability distributions, we design an inverse problem that (1) is overdetermined and computationally efficient because the image is described by only a few parameters, (2) produces tomograms consistent with expected plume behaviour (e.g. changes of one sign relative to the background image), (3) yields parameter estimates that are readily interpreted for plume morphology and offer direct insight into hydrologic processes and (4) requires comparatively few data to achieve reasonable model estimates. We demonstrate the approach in a series of numerical examples based on straight-ray difference-attenuation radar monitoring of the transport of an ionic tracer, and show that the methodology outlined here is particularly effective when limited data are available.

Key words: Image processing; Inverse theory; Ground penetrating radar; Hydrogeophysics.

1 INTRODUCTION

Recent advances in geophysical instrumentation, inversion approaches and software have enabled unprecedented insights into diverse, natural and engineered hydrologic processes including transport of ionic tracers (e.g. Slater *et al.* 1997; Kemna *et al.* 2002; Day-Lewis *et al.* 2003; Vanderborght *et al.* 2005; Cassiani *et al.* 2006; Day-Lewis *et al.* 2006; Singha & Gorelick 2006), infiltration (e.g. Binley *et al.* 2001; Deiana *et al.* 2008; Looms *et al.* 2008a,b; Nimmo *et al.* 2009), submarine groundwater discharge (Swarzenski *et al.* 2006, 2007; Nguyen *et al.* 2009; Henderson *et al.* 2010), aquifer storage and recovery (Singha *et al.* 2007) and *in situ* engineered aquifer remediation (e.g. Lane *et al.* 2004; Williams *et al.* 2005; Lane *et al.* 2006; Hubbard *et al.* 2008; Chen *et al.* 2009; Williams *et al.* 2009; Johnson *et al.* 2010). In much of this work, difference tomographic imaging is used to produce tomograms that are interpreted as 'snapshots' of changes to pore-fluid properties through time (e.g. Kemna *et al.* 2006). The ability of difference tomography to resolve a plume—or any target—depends on (1) the physics underlying the measurements (e.g. electrical conduction or seismic wave propagation) and approximations made in the forward model for inversion, (2) the survey geometry and acquisition rate, which are commonly limited in geophysical problems, (3) the measurement errors, (4) the parametrization of the inverse problem, (5)

the regularization criteria, if any, used to make the problem well posed and (6) other prior information used in the inversion. The resolving power of tomography is a well-studied problem (Backus & Gilbert 1968; Menke 1984; Friedel 2003; Sheng & Schuster 2003; Day-Lewis & Lane 2004; Day-Lewis *et al.* 2005), but relatively little attention has been paid in the literature to the particular problem of dynamically imaging plumes.

Plumes commonly are described by hydrologists in terms of their statistical moments (e.g. Freyberg 1986; Goltz & Roberts 1987; Adams & Gelhar 1992; Cirpka & Kitanidis 2000). Indeed, plumes undergoing advective–dispersive transport in homogeneous media follow a Gaussian distribution in space and time (depending on boundary conditions), where the centres of mass are controlled by advection and the standard deviation by dispersive spreading. Description of more complicated plumes requires use of higher order moments (e.g. skewness, kurtosis; Harvey & Gorelick 2000). Moments or probability distributions provide an appealing and natural parametrization for inversion of difference tomograms of plumes, in that few parameters are required to describe the distribution. In principle, geophysical data can be used to infer plume characteristics (e.g. total mass, centre of mass, spread, tailing), which in turn provide insight into hydrologic processes (i.e. advection, dispersion, decay and rate-limited mass transfer). For example, in laboratory experiments, Slater *et al*. (2000) used time-lapse electrical resistivity tomography (ERT) to estimate tracer breakthrough curves for different pixels during saline tracer transport in a tank. In field applications, however, attempts to calculate plume moments from time-lapse tomograms commonly have produced spurious results. In an application of time-lapse ERT to monitor a fluid tracer in the unsaturated zone, Binley *et al.* (2002) observed a 50 per cent discrepancy between the injected mass and the mass recovered by ERT; this mass-balance error was attributed to variable ERT sensitivity and poor resolution of tracer in portions of the tomogram. Similarly, in an application of ERT to monitor a saline tracer, Singha & Gorelick (2005) noted a similar underestimate in mass and an overestimate in spatial variance due to regularization and inversion artefacts.

Recently, Day-Lewis *et al*. (2007) derived a new 'moment resolution matrix' to predict the moments of an image as a function of the plume's true moments while accounting for the measurement physics, survey geometry and regularization criteria, as described by the inverse problem's conventional model resolution matrix (Menke 1984). Day-Lewis *et al*. (2007) demonstrated that plume moments inferred from tomograms are strongly affected and potentially biased by the regularization employed, with the choice of regularization criteria largely arbitrary and subjective. Furthermore, the reliability of inferred moments depends on where the plume lies in the image plane because resolving power varies over a tomogram as a complicated function of survey geometry and measurement physics. These problems arise from the fact that most tomographic inverse problems in geophysics are underdetermined and require regularization to make well posed and soluble. Regularization entails additional inversion constraints to produce the simplest image consistent with the data, where simplicity is defined variously in terms of uniformity, flatness, or smoothness, which, respectively are quantified by deviation from a mean value, minimization of the first spatial derivative, or minimization of the second spatial derivative (Tikhonov & Arsenin 1977).

We contend that common parametrizations and regularization criteria (uniformity, flatness, smoothness) do not leverage our *a priori* understanding of expected plume morphology and the physics underlying transport processes. Although solutions using regularization schemes, such as those described by Tikhonov & Arsenin (1977) for pixelated images, can result in reasonable estimates of plume parameters, they require substantial data to do so. One major limitation with difference geophysics is that data collection is constrained in time by changes to the image; that is, the image is changing during data collection yielding an unfortunate trade-off between temporal smearing and data coverage.

Furthermore, when applied to difference tomography, regularization strategies can produce images of plumes with streaks and artefacts of opposite sign to that expected (e.g. Day-Lewis *et al.* 2002), where the regularization seeks to balance, for example, the positive anomaly represented by the plume with framing, spurious negative anomalies. Although damping regularization leads to underestimation of total mass, smoothness and flatness criteria tend to produce plumes that are overly diffuse (Singha & Gorelick 2005; Day-Lewis *et al.* 2007). The shortcomings of pixel-based parametrization and conventional regularization strategies are well understood, particularly in the context of static imaging. A number of alternative parametrizations have been proposed in the literature, including natural pixels (e.g. Buonocore *et al.* 1981; Michelena & Harris 1991), geometric objects (e.g. Miller *et al.* 2000; Lane *et al.* 2004, 2006), statistical moments (e.g. Milanfar *et al.* 1996) and level sets (e.g. Dorn *et al.* 2000). The philosophies underlying these parametrizations differ, with some designed to capitalize on the measurement configuration and physics (e.g. natural pixels), and others to take advantage of knowledge of the imaged target (e.g. moments, geometric objects). Underlying these efforts are objectives of (1) reducing the number of inversion parameters, thus facilitating rapid time-lapse or 3-D imaging (e.g. reducing both acquisition and inversion time), (2) matching the inversion parameters to quantities of engineering or geological relevance (e.g. anomaly centre of mass, magnitude and size), thus facilitating use of inversion results by non-geophysicists and (3) defining parameters that reduce the need for regularization and prevent the inversion from producing spurious anomalies inconsistent with the structure under study. In the context of plume imaging, the ideal parametrization would describe plumes fully and accurately using as few parameters as possible; furthermore, non-physical plumes (e.g. plumes showing mass loss in 3-D when conservation is expected) would be excluded from the solution space by virtue of the parametrization, obviating regularization.

Of particular relevance to our current effort is the work of Milanfar *et al*. (1996), who described an image in terms of orthogonal Legendre moments, which are related algebraically to the conventional geometric moments (e.g. centre of mass, spread) used to describe plumes. For the case of ray-projection data, Milanfar *et al*. (1996) formulated a tomographic inverse problem as estimation of spatial moments. Image moments provided a compact parametrization resulting in an overdetermined inverse problem. Here, we adapt this idea and propose a parametrization based on probability-distribution descriptors; hence our inversion parameters are the distribution's parameters (e.g. mean, standard deviation). This formulation is appealing for tomographic imaging of plumes because distribution parameters provide direct insight into the physical processes controlling plume morphology. For example, the location of a plume's centre of mass is controlled by advection, and its spatial spread is controlled by dispersion. By assuming a specific distribution, we also impose additional constraints (i.e. insight) on the inversion, with one important constraint being that the image should be positive-valued. Importantly, the method outlined here performs well in the presence of limited data.

2 APPROACH

2.1 Distribution-based parametrization

In this work, we demonstrate the use of a distribution-based parametrization for difference-tomography monitoring of plumes associated with solute or mass transport. Although we demonstrate our approach for straight-ray radar difference-attenuation data, the inversion approach is general. The approach is based on a distribution-based parametrization, in which the tomographic image is described by eight parameters (Fig. 1): (1) the plume mass, M; (2, 3) centre of mass in the x and z locations in Cartesian coordinates, μ_x and μ_z; (4, 5) the standard deviation in the x and z directions, σ_x and σ_z; (6, 7) two windowing lengths WL_x and WL_z that allow only part of the distribution to be used to describe the plume shape and (8) a rotation angle from horizontal, θ. The windowing lengths truncate the distribution, and are used to tailor the shape of subsurface plumes. These provide additional flexibility to describe plumes that take on zero values or have sharp peaks, which cannot exist in purely Gaussian or lognormal distributions. These lengths are particularly useful with the lognormal distribution, where adjusting either the centre of mass or spatial variance changes the shape of the plume such that it would be more or less disperse. These lengths have a magnitude between zero and one, where one indicates minimal truncation, and zero would be entirely truncated, that is, zero-valued. In contrast to the orthogonal moments of Milanfar *et al.* (1996), the distribution parameters considered here are correlated.

2.1.1 Creating a parameter field

A distribution must be assumed to use this methodology, entailing an assumption of the target's morphology (i.e. we invoke *a priori* knowledge about the problem). The framework presented here is flexible and diverse parametric distributions (Gaussian, lognormal, gamma) are possible. These types of parametrizations should not be considered one-size-fits-all, they should be thought of as problem-specific. For tracer transport, Gaussian distributions commonly cannot describe field observations adequately; most studies of solute transport show extended tailing in concentration in space and time as a function of heterogeneity (e.g. Grisak *et al.* 1980; Becker & Shapiro 2000; Harvey & Gorelick 2000; LaBolle & Fogg 2001; Meigs & Beauheim 2001; Gorelick *et al.* 2005). To demonstrate our approach, we use two distribution-based parametrizations. The first is based on the bivariate Gaussian distribution

$$f\left(x_{\mathrm{G1}}, x_{\mathrm{G2}}\right) = \frac{1}{2\pi\,\sigma_{\mathrm{G1}}\,\sigma_{\mathrm{G2}}} \left\{ \exp^{-\frac{1}{2}\left[\frac{(x_{\mathrm{G1}}-\mu_{\mathrm{G1}})^2}{\sigma^2_{\mathrm{G1}}} + \frac{(x_{\mathrm{G2}}-\mu_{\mathrm{G2}})^2}{\sigma^2_{\mathrm{G2}}}\right]} \right\}, \quad (1)$$

where μ_{G1} and μ_{G2} are the centre of mass in the x_{G1} and x_{G2} directions, and σ_{G1} and σ_{G2} are the standard deviations in x_{G1} and x_{G2}. The directions x_{G1} and x_{G2} are the principal directions of the 2-D bivariate distribution but are not necessarily aligned with the x and z axes of the experimental pixelated grid; that is, the x_{G1}–x_{G2} grid can be rotated about the experimental grid. To allow for long tailing, we introduce a distribution that is Gaussian in one direction (x_{G1}), but the lognormal in the other (formerly x_{G2}, now x_{LN2})

$$f(x_{\mathrm{G1}}, x_{\mathrm{LN2}}) = \frac{1}{2\pi\, x_{\mathrm{LN2}} \sigma_{\mathrm{G1}} \sigma_{\mathrm{LN2}}} \left\{ \exp^{-\frac{1}{2}\left[\frac{(x_{\mathrm{G1}}-\mu_{\mathrm{G1}})^2}{\sigma^2_{\mathrm{G1}}} + \frac{[\log(x_{\mathrm{LN2}})-\mu_{\mathrm{LN2}}]^2}{\sigma^2_{\mathrm{LN2}}}\right]} \right\}, \quad (2)$$

where μ_{G1} and μ_{LN2} are the mean in the x_{G1} and x_{LN2} directions, and σ_{G1} and σ_{LN2} are the standard deviations in x_{G1} and x_{LN2}, respectively. With the use of a rotation angle, we need not assume in which direction (in x or z) the lognormal tailing should occur.

To create an initial and subsequent parameter distribution for forward modeling, we use the following algorithm (Fig. 1):

(1) Declare a model vector, **m**, which is comprised of the eight distribution parameters outlined above.

(2) Define a numerical grid from 0 to $\mathrm{WL}_{\mathrm{LN}}$ in the lognormal direction if a lognormal distribution is used, and from $-\mathrm{WL}_{\mathrm{G}}$ to WL_{G} in the Gaussian direction(s). The number (and size) of the cells in the numerical grid will be governed by the underlying forward problem and will typically need to strike a balance between computational expedience with numerical accuracy.

(3) Evaluate either eq. (1) or (2) on the grid defined in ii, assuming a centre of mass of 0 for the Gaussian component(s) and a centre of mass of 0.1 for the lognormal component. Because the shape of the lognormal distribution changes as a function of the centre of mass, we make an arbitrary decision to fix the initial estimate at 0.1. The distribution is then translated and rotated as described below. Other values could be used, resulting in differently shaped distributions; multiple shapes could be considered.

(4) Interpolate the distribution onto the experimental grid to generate the image field, **p**, consisting of a discretized (pixelated) image of the geophysical parameter. Rotate the resulting field as denoted by the angle included in the model vector, and translate the plume parametrization (by the centre of mass in x and z) as needed. Normalize the image field **p** on the experimental grid so the total mass of the grid is equal to the mass specified in the model vector.

The forward operator can be applied to the resulting image field, **p**, to calculate the forward response of the experiment. We calculate the moments of the parameter field directly from the discretized distributions in the experimental grid.

2.1.2 Distribution-based inversion

We can formulate a forward problem to calculate the predicted data, $\mathbf{d}_{\mathrm{pred}}$, given our distribution parameters, **m**, which first are translated into the image field **p**

$$\mathbf{Ap}(\mathbf{m}) = \mathbf{d}_{\mathrm{pred}}, \quad (3)$$

where **A** represents our forward-modeling operator and $\mathbf{d}_{\mathrm{pred}}$ is our predicted data vector for a given **m**. For the straight-ray attenuation tomography problem used here for illustration, **p** is difference attenuation, that is, α^i–α^0, where α^i is the vector of pixelated attenuation at time i and α^0 is the vector of pixelated background attenuation before injection of solute. The data, $\mathbf{d}_{\mathrm{obs}}$, would be taken as ratios of the logarithms of peak-to-peak amplitudes (or trace energy) for data sets from time i and background (e.g. Day-Lewis *et al.* 2003).

It is evident from (3) that even if the forward model is described by a linear operation on **p**, it will not be a linear operation on **m**. Consequently, the distribution-based inversion is also non-linear. Given (3), we seek to recover the model vector, **m** (which is shown in step 1 of Fig. 1), that results in the parameter field, **p**, that best describes our observed data. To do this, we formulate the following objective function, which we minimize in the least-squares sense:

$$\Phi(\mathbf{m}) = \left\| \mathbf{W}_{\mathrm{d}} \left[\mathbf{d}_{\mathrm{obs}} - \mathbf{Ap}(\mathbf{m}) \right] \right\|^2, \quad (4)$$

where $\mathbf{d}_{\mathrm{obs}}$ is our measured field data and $\mathbf{W}_{\mathrm{d}}$ is a diagonal matrix that contains the inverse of the standard deviation of the data.

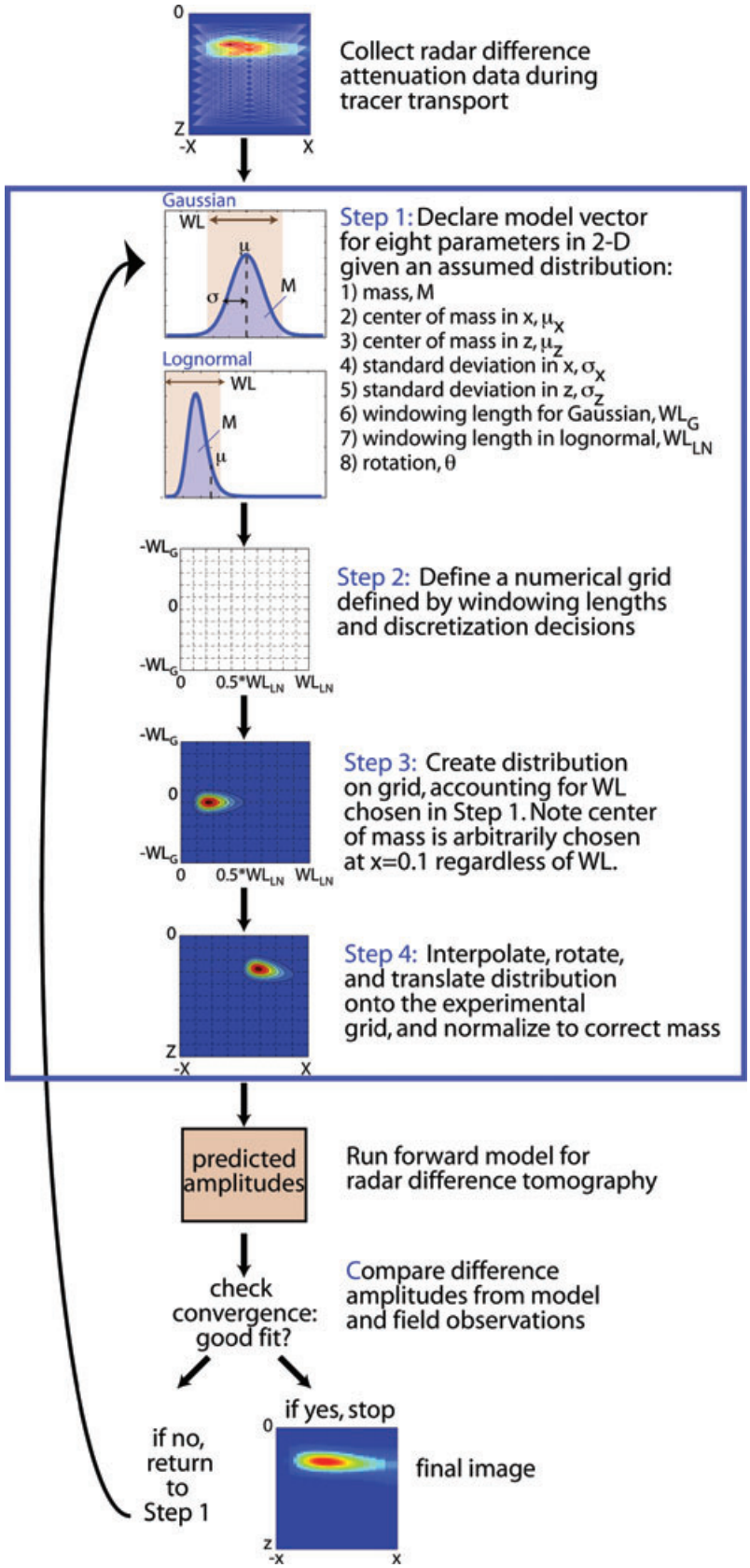

Figure 1. Flowchart of parametrization and inversion procedure.

Given that this problem is well posed, we do not require regularization terms in the objective function. We do, however, apply constraints to each of the model parameters. For lower bounds, we know that all the parameters are greater than zero, assuming the experimental coordinate system starts at (0, 0) and that the centre of mass is within our experimental grid. For upper bounds, we can use our understanding of our field system to estimate an upper bound for mass, centre of mass and standard deviations. Similarly, we know that the angle of rotation cannot exceed 2π for an asymmetric plume, which would be the case if one of the axes in the distribution is lognormal. Given these constraints, we solve eq. (4) using a trust-region-reflective optimization algorithm (lsqnonlin) in MATLAB (Coleman & Li 1996). This implementation is only suitable for problems with a small number of parameters, as it relies on a perturbation approach to estimating the sensitivity matrix used in the optimization.

Presented in Fig. 1 is a workflow of our parametrization/inversion process for the case of radar-attenuation tomography, including the four-step algorithm outlined earlier. First, we simulate radar attenuation data during a tracer transport test. Next, we choose a distribution for our parametrization, and evaluate this model for a starting guess **m** as described below (Step 1). From the eight parameters and the mathematical model for the distribution, we generate our parameter field as outlined in the algorithm above (Step 2–4). Given this field, we evaluate eq. (3) to predict the data, which are compared to the observations. If the difference between the estimated and observed data is below a given tolerance, the algorithm has converged; otherwise, **m** is updated, and the system is repeated until convergence.

2.2 Traditional least-squares inversion

To provide a basis for comparison, we also test a traditional least-squares inversion routine to recover our parameter field. For straight-ray difference-attenuation radar tomography, we consider the following forward problem:

$$\mathbf{A}\Delta\alpha = \Delta\mathbf{a}, \tag{5}$$

where $\mathbf{A}$ is a matrix that contains the length a ray traverses in each cell, $\Delta\alpha$, is vector representing the difference amplitudes between the k-time data set and the background data set, and $\Delta\mathbf{a}$ is the ratio of the logarithms of amplitudes (e.g. peak-to-peak) between the k-time data set and the background data set. To recover the attenuation vector $\Delta\mathbf{a}$, for a given time step, we solve the following linear inverse problem:

$$\Delta\alpha = \left(\mathbf{A}^T\mathbf{W}_\mathbf{d}^\mathbf{T}\mathbf{W}_\mathrm{d}\mathbf{A} + w_\mathrm{x}\cdot\mathbf{W}_\mathbf{x}^\mathbf{T}\mathbf{W}_\mathrm{x} + w_z\cdot\mathbf{W}_\mathbf{z}^\mathbf{T}\mathbf{W}_\mathbf{z} + w_\mathrm{s}\cdot\mathbf{I}\right)^{-1} \times \left(\mathbf{A}^T\mathbf{W}_\mathbf{d}^\mathbf{T}\mathbf{W}_\mathrm{d}\Delta\mathbf{a}\right), \tag{6}$$

where $\mathbf{W}_x$ and $\mathbf{W}_z$ are first-order difference operators in the x and z directions, respectively; w_x and w_z are weighting parameters in the x and z directions, with larger values promoting smoothness in a given direction; w_s is a weighting parameter to enforce model smallness and to stabilize the inversions. For the result presented here, values for w_x and w_z were 100 and 10, respectively. w_s was taken to be 0.001. These values were chosen from a suite of possible regularization terms; the increased smoothing in the x-direction with respect to the z-direction is because of *a priori* knowledge of the plume migration in x. The smallness term was set to a minimal value to stabilize the inversion without impacting the subsequent inversions.

2.3 Calculating moments

After calculating the parameter field, **p**, that best describes our observed data via least-squares inversion or the alternative parametrization [i.e. **p(m)**] outlined above, a tomogram is reconstructed for the tracer experiment at each time step. Once a satisfactory fit to the data has been achieved, we calculate spatial moments on the reconstructed image for interpretation of plume morphology and transport behaviour. We estimate spatial moments from these tomograms according to

$$M_{ij}(t) = n\iint_\Gamma \mathrm{conc}(x,z,t)x^i z^j \mathrm{d}x\mathrm{d}z, \tag{7}$$

where M_{ij} is the spatial moment of interest; i, j are exponents with values from 0 to 2, whose value(s) depend on the particular moment of interest; n is the effective porosity; conc is the concentration [derived from either **p(m)** or $\Delta\alpha$] in mg L^{-1}; x, z are Cartesian coordinates; dx, dz are the voxel dimensions in the x and z directions, and Γ is the test domain within the area of interest. The zeroth moment, M_{00}, is the mass in the system. The first moment (M_{10}, M_{01}) normalized by the mass, defines the centre of mass of the tracer in each principal direction. The variance or covariance of the tracer plume (spread and rotation) is related to the second spatial moment (M_{20}, M_{02}, M_{11}), centre of mass, and tracer mass as

$$\sigma_x = \sqrt{\frac{M_{2,0}}{M_{0,0}} - \left(\frac{M_{1,0}}{M_{0,0}}\right)^2} \text{ and} \tag{8a}$$

$$\sigma_z = \sqrt{\frac{M_{0,2}}{M_{0,0}} - \left(\frac{M_{0,1}}{M_{0,0}}\right)^2}. \tag{8b}$$

It should be noted that our example problems are based on linear difference-attenuation tomography. By analysing differences from a background data set, we invert directly for temporal differences associated only with the injected plume. In practice, the straight-ray assumption may be violated by geological heterogeneity or as a result of injections, thus requiring a non-linear inversion for slowness before (or joint with) inversion for difference attenuation. In applications to electrical resistivity tomography, our approach could be applied to difference (or ratio) data to invert for difference electrical conductivity. Alternatively, the inversion could be designed to estimate changes from a background image produced previously by an independent inversion.

3 NUMERICAL EXAMPLES

We demonstrate our methodology for two cases: (1) a base case with advective–dispersive transport and (2) a highly advective case with low dispersion. In both cases, we use a heterogeneous hydraulic conductivity field built from a binary system of 10 and 100 m d^{-1} with a constant porosity of 0.1, representative of a fluvial wash. Steady-state groundwater flow is simulated on a 32 pixel × 36 pixel grid with pixels 0.5 m on a side in the area of interest using MODFLOW-2000 (Harbaugh *et al.* 2000) and transient transport is simulated using MT3DMS (Zheng & Wang 1999). We assume no-flow/no-flux boundaries at the top and bottom and fixed-head/fixed-concentration boundaries on the left and right sides such that a lateral head gradient of 0.02 is produced and the concentration is fixed to the background value of 100 mg L^{-1}. A 1000 mg L^{-1} tracer is injected within a well 3 m long located on the left side of the grid. A dispersivity of 2 m is assumed in the longitudinal direction. In the

high-advection case, the dispersivity in the longitudinal direction is dropped to 0.1 m. The tracer is monitored over 8 d.

Concentration data are converted to electrical conductivity at each time step using Archie's law (Archie 1942),

$$s_b = 1/F s_f, \tag{9}$$

where s_b is the bulk electrical conductivity (S m^{-1}), s_f is the fluid electrical conductivity (S m^{-1}) and F is the formation factor, which is a function of the effective porosity and connectivity of the pore space (Guyod 1944), and here assumed to be equal to five. Concentration data are converted to attenuation values using the high-frequency approximation where

$$\Delta\alpha = 1.68 \times 10^3 \Delta s_b \frac{v}{c}, \tag{10}$$

where $\Delta\alpha$ is the attenuation in dB, v is the EM-wave propagation velocity in the medium, assumed to be 6×10^7 m s^{-1} and c is the speed of light in a vacuum. Given the estimated attenuation, we simulate straight-ray radar tomography with borehole radar wells on the boundary of the grid. We run forward models with 1600 and 100 data (we refer to these as the 'dense' and 'sparse' data options, respectively; see Fig. 2) to demonstrate how the alternative distribution-based parametrization performs with limited data in comparison to a standard overparametrized least-squares inversion. We assume Gaussian random errors with a standard deviation of 3 per cent of the measurements, as could arise from picking error and minor errors in well-assumed deviations. Here, we explore the accuracy of the distribution-based parametrization described above with respect to classical least-squares inversion for three different cases with varying amounts of data.

For the cases presented, we assume a starting model where the centre of mass is at the centre of the experimental grid. The initial standard deviation is assumed to be half the grid width, meaning that the entire grid would be spanned within one standard deviation. The rotation angle is initially estimated to be 0, but is free to vary between 0 and 2π.

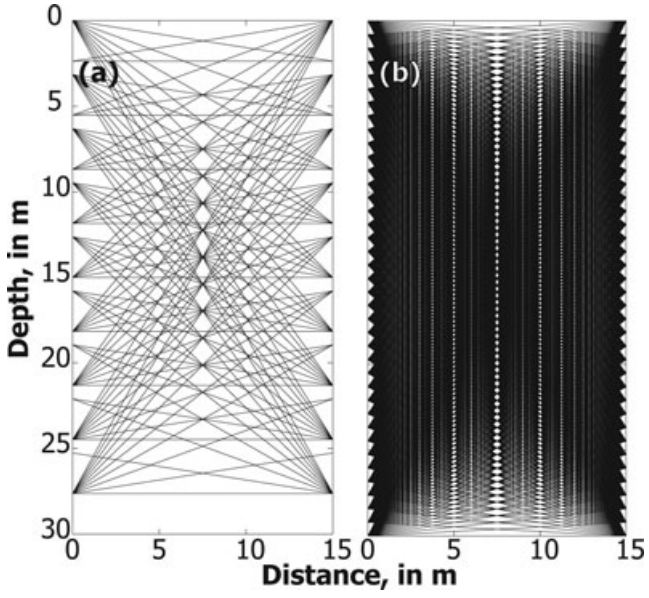

Figure 2. Data coverage for (a) 100 and (b) 1600 measurement cases.

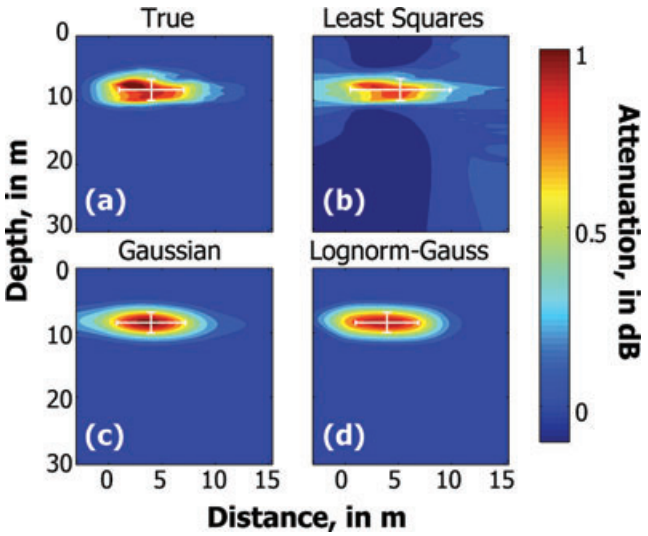

Figure 3. (a) The true concentration plume for Case 1 (the base case) from a time 2 d after injection and associated reconstructed images given 1600 radar traveltime data for the (b) standard least-squares inversion, (c) alternative parametrization based on a Gaussian plume, (d) alternative parametrization based on a plume defined by a Gaussian distribution in one direction and a lognormal distribution in the other. The mean and variance of the plumes are shown on each subplot in white lines.

3.1 Case 1: advection–dispersion

The inversion of attenuation data based on an advecting, dispersing conductive tracer, given 1600 measurements, is shown in Fig. 3. In the case of many data, the least-squares inversion (Fig. 3b) qualitatively maps the true case (Fig. 3a) closely, although streaking and smearing of the estimated plume is apparent in the tomogram. In addition, some negative values appear in the reconstruction. The tomograms based on our alternative parametrization, including that based on a Gaussian distribution (Fig. 3c) and the combined lognormal-Gaussian distribution (Fig. 3d), do not show the same artefacts or negative values, although are limited by their simpler parametrization so they cannot map the plume irregularities exactly. The strength of alternative parameterizations becomes clearer with limited data (Fig. 4). When we reduce from 1600 measurements to 100, the least-squares inversion performs notably more poorly, especially with respect to capturing the high-attenuation areas of the tomogram (Fig. 4b), whereas the alternative parametrizations are still able to map the magnitude of tracer plume reasonably accurately. The shape and mass of the tracer plume remains well captured when compared to the least-squares case, although the models are too simple to describe the distribution exactly.

When we consider spatial moments, we find that the alternative parametrizations shown here generally better identify properties, especially in the case of limited data (Fig. 5). The Gaussian and lognormal-Gaussian models perform similarly well in most cases, except when estimating the variance in the x-direction, where the Gaussian model does not perform as well; we attribute this to the model's inability to capture any tailing behaviour with this simplified parametrization.

Because of negative values of attenuation, calculating moments on the traditional least-squares case is problematic; whereas the estimate of total mass and centre of masses are accurate when summing over the plane, high values are countered by negative values in portions of the tomogram produced from traditional least squares. Negative mass, which is clearly non-physical, can result in negative

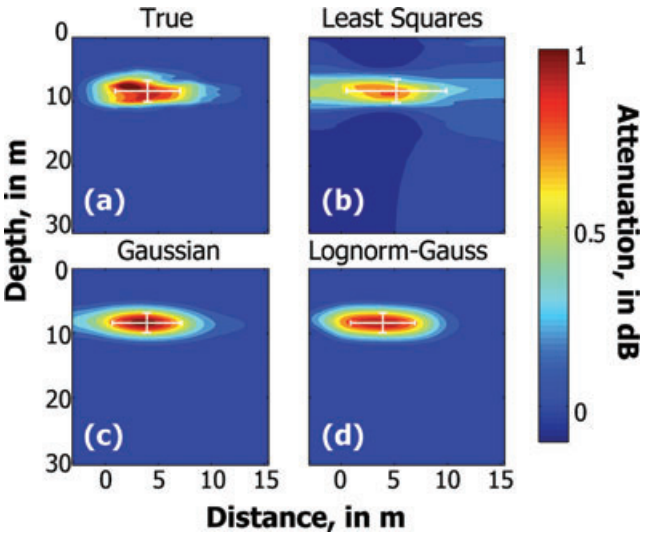

Figure 4. (a) The true concentration plume for Case 1 (the base case) from a time 2 d after injection and associated reconstructed images given 100 radar traveltime data for the (b) standard least-squares inversion, (c) alternative parametrization based on a Gaussian plume, (d) alternative parametrization based on a plume defined by a Gaussian distribution in one direction and a lognormal distribution in the other. The mean and variance of the plumes are shown on each subplot in white lines.

spatial variance when using eq. (8). With fewer data we find that at all times for all moments, the alternative parametrizations perform as well, if not better than the standard least-squares inversion. These tomograms are not affected by streaking and related artefacts.

3.2 Case 2: highly advective case

We consider one additional test case, where the dispersivity is notably less than in the first case (0.1 m in the longitudinal direction, as compared to 2 m). This creates a less diffuse plume that shows some fingering as a function of the heterogeneity in hydraulic conductivity (Fig. 6a); this shape is particularly hard for geophysical imaging to capture due to the high contrast and small size. This shape is not well described by either a Gaussian or lognormal-Gaussian distribution; parametrizations based on these shapes do not capture the shape well (Figs 6c and d).

With 1600 data, the least-squares inversion is able to capture the general shape (Fig. 6b), but with notable artefacts and streaking in the tomogram. As in the previous cases, the examples with 100 data indicate the strength of the methodology considered here: although the tomograms themselves do not capture the correct shape with any of the parametrizations shown (Figs 7c and d), the least-squares inversion is particularly impacted by streaks and negative attenuation values, and does a poor job of mapping the areas of highest attenuation (Fig. 7b). Regardless of data, the moments show that the least-squares inversion performs slightly better than the alternative parametrizations with respect to μ_z and σ_z^2 (Fig. 8). The tracer moves more quickly in this case than in the previous one, so after 3.5 d, the tracer is largely absent from the 2-D simulation plane; moments after this time are not meaningful as they are more sensitive to the presence of noise in the system than data. With sparse data, all parametrizations provide poor representations of the true system. The alternative parametrizations still capture mass and centre of mass reasonably well, especially at early time, but errors in spatial variance and skewness are high in all cases.

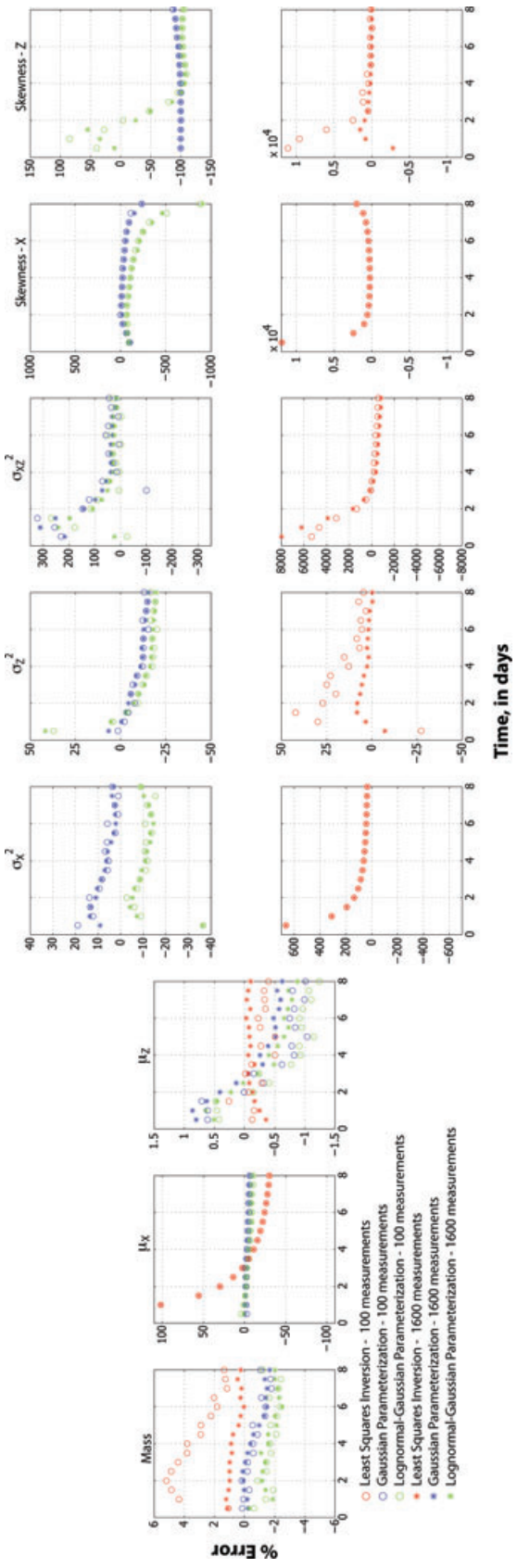

Figure 5. Per cent error in mass, centre of mass, spatial variance and skewness from the true values for the reconstructed tomograms for Case 1, the base case model. Note that the alternative parametrizations are plotted with smaller *y*-axes than the least-squares inversion for variance and skewness.

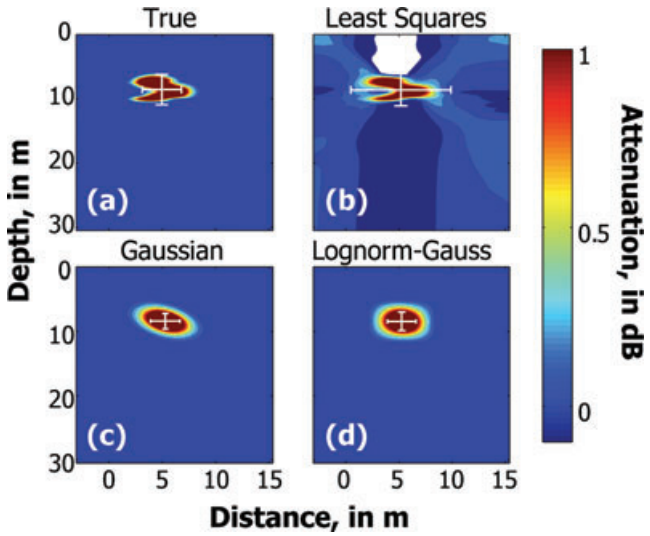

Figure 6. (a) The true concentration plume for Case 2 (the highly advective case) from a time 1-d after injection and associated reconstructed images given 1600 radar traveltime data for the (b) standard least-squares inversion, (c) alternative parametrization based on a Gaussian plume, (d) alternative parametrization based on a plume defined by a Gaussian distribution in one direction and a lognormal distribution in the other. The mean and variance of the plumes are shown on each subplot in white lines. The white area in the least-square tomogram has attenuation values less than −0.1 dB.

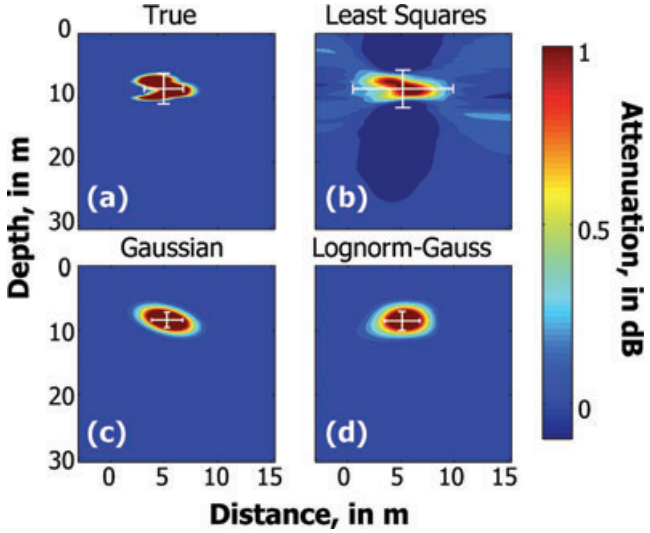

Figure 7. (a) The true concentration plume for Case 2 (the highly advective case) from a time 1-d after injection and associated reconstructed images given 100 radar traveltime data for the (b) standard least-squares inversion, (c) alternative parametrization based on a Gaussian plume, (d) alternative parametrization based on a plume defined by a Gaussian distribution in one direction and a lognormal distribution in the other. The mean and variance of the plumes are shown on each subplot in white lines.

4 DISCUSSION AND CONCLUSIONS

We presented a novel parametrization for difference tomographic imaging of hydrologic processes based on a simple analogy between plume morphology and probability distributions. Numerical examples demonstrated the advantages of our distribution-based parametrization over conventional pixel-based parametrization using smoothness-based regularization, especially in the presence of limited data. Although the conventional approach yielded biased

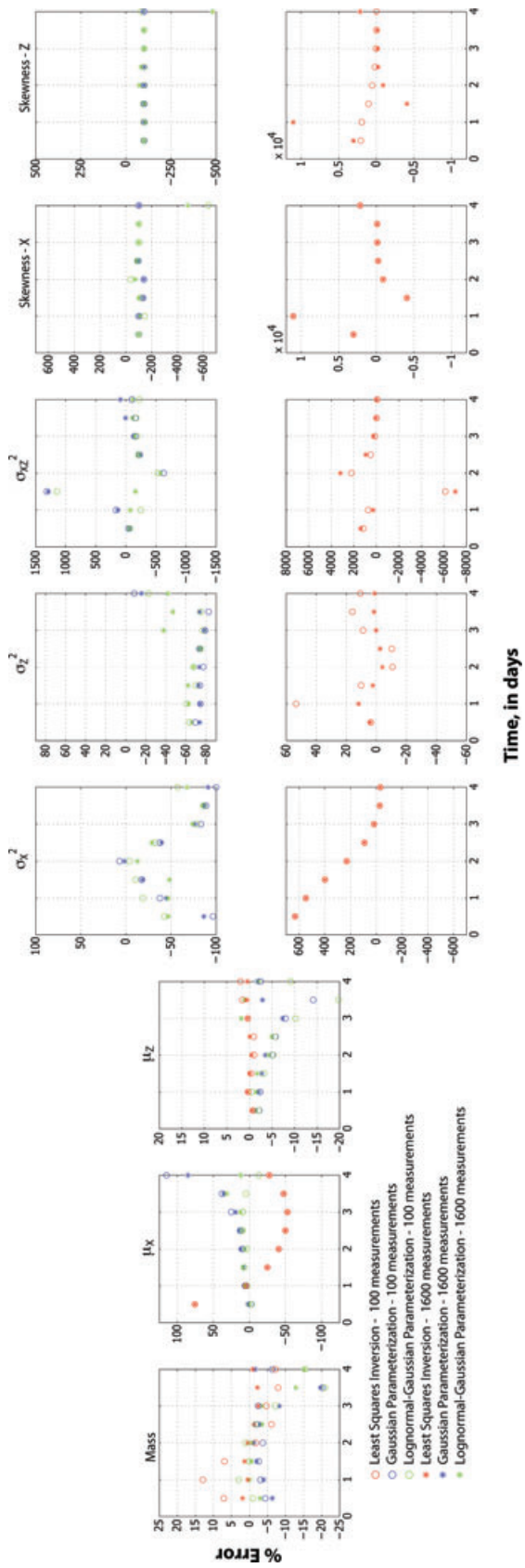

Figure 8. Per cent error in mass, centre of mass, spatial variance and skewness from the true values for the reconstructed tomograms for Case 2, the model that is highly advective. Note that the alternative parametrizations are plotted with smaller *y*-axes than the least-squares inversion for variance and skewness.

estimates of plume moments in many cases (i.e. underprediction of total mass, overprediction of spreading) and was greatly impacted by artefacts, our approach yielded reliable moment estimates and was robust in the presence of sparse data. The negative values of attenuation estimated from least-squares inversion often lead to accurate estimates of total mass or centre of mass when summing over the plane, but this was because high values are countered by negative values. In addition, spatial variances calculated on the least-squares inversion were frequently negative as a result of the least-squares inversion's indication of negative concentration (i.e. decrease in attenuation from background). These problems were negated with the alternative parametrizations described here. The fact that our alternative parametrization cannot include these negative values, or artefacts, highlights another potential advantage of this approach or a non-linear least-squares inversion (e.g. curved ray), in that we are not faced with the challenge of choosing when to stop an inversion. With the parametrization-based approach we can iterate until the model no longer changes; because the model has no capacity to include artefacts, there is no penalty for overiteration unlike with a non-linear least-squares approach. We also note that the problem considered here represents an ideal scenario with respect to inversion using standard least squares, in so much as our model space is small and, therefore, better determined than would normally be the case; moreover, we use the same computational grid for the forward and inverse solutions.

The distributions considered here are described by only a few parameters, so the resulting inverse problems are overdetermined and computationally efficient to solve. Extension of our 2-D parametrization to 3-D or 4-D (3-D plus time) is possible and should allow for application to large time-lapse problems. Importantly, the inverse problem for our parametrization scales efficiently with dimensionality, with 8 parameters for 2-D, 13 parameters for 3-D and 19 parameters for 4-D (assuming parameters that describe migration and spreading in three principal directions). For comparison, pixel-based inverse problems would require N^2, N^3 and N^3T parameters for 2-D, 3-D and 4-D, respectively, assuming N pixels in each direction and T time steps. We note, that the extension to the 4-D problem is different from the 2-D plus time formulation we have presented here. In an explicit 4-D parametrization, the time variance of the system can be included in the formulation of the model, as such. We solve the problem simultaneously for all time steps. Also of importance is that for the cases outlined here, the final model parameters are largely insensitive to the starting model. We explored multiple starting guesses, and found for the case of attenuation tomography, convergence is minimally sensitive to these initial guesses. Although synthetic cases are demonstrated here, application to field data should be straightforward, and complicated only by a non-constant background fluid conductivity. In the examples presented, we analyse differences from a background data set, meaning that we focus on changes and, therefore, should be sensitive only to the injected plume. The major limitation to the work presented here is the straight-ray assumption, which may be violated by geological heterogeneity or as a result of injections; however, this can be easily handled by including another iteration loop in the inversion that updates the ray paths in **A**, based on the new **m**, as is performed on inversions considering fat rays (e.g. Day-Lewis *et al.* 2005; Johnson *et al.* 2005, 2007) or full-waveform inversion (e.g. Ernst *et al.* 2007). Alternatively, the inversion could be designed to estimate changes from a background image produced previously by conventional least-squares inversion as a starting point.

Although we considered only Gaussian and lognormal distributions, consideration of other probability distributions, or modifications to the distributions presented here (e.g. changing of the windowing approach), is possible. Other models may lead to improved recovery of the properties describing plume transport. Consideration of, for example, gamma distributions may allow for description of more complicated plumes that exhibit strong tailing behaviour. Extension of the framework here to other distribution types—possibly with more parameters and capable of describing complex plumes—is straightforward. The methodology presented here should be widely applicable to mapping tracer plume locations in 2-D and 3-D, and useful for mapping the behaviour of plume transport in field settings.

ACKNOWLEDGMENTS

This material is based upon work supported by the National Science Foundation Grant EAR-0747629 and by the U.S. Geological Survey Toxic Substances Hydrology Program. Any opinions, findings and conclusions or recommendations expressed in this material are those of the authors and do not necessarily reflect the views of the National Science Foundation. The authors are grateful to Rory Henderson and Seth Haines for comments on an early draft of the manuscript.

REFERENCES

Adams, E.E. & Gelhar, L.W., 1992. Field study of dispersion in a heterogeneous aquifer. 2. Spatial moments analysis, *Water Resour. Res.,* **28,** 3293–3307.

Archie, G.E., 1942. The electrical resistivity log as an aid in determining some reservoir characteristics, *Trans. Am. Inst. Min. Metall. Pet. Eng.,* **146,** 54–62.

Backus, G.E. & Gilbert, J.F., 1968. The resolving power of gross earth data, *Geophys. J. R. astr. Soc.,* **16,** 169–205.

Becker, M.W. & Shapiro, A.M., 2000. Tracer transport in fractured crystalline rock: evidence of nondiffusive breakthrough tailing, *Water Resour. Res.,* **36,** 1677–1686.

Binley, A., Winship, P., Middleton, R., Pokar, M., & West, J., 2001. High-resolution characterization of vadose zone dynamics using cross-borehole radar, *Water Resour. Res.,* **37,** 2639–2652.

Binley, A., Cassiani, G., Middleton, R. & Winship, P., 2002. Vadose zone flow model parameterisation using cross-borehole radar and resistivity imaging, *J. Hydrol.,* **267,** 147–159.

Buonocore, M.H., Brody, W.R. & Macovski, A., 1981. A natural pixel decomposition for two-dimensional image reconstruction, *IEEE Trans. Biomed. Eng.,* **28,** 69–78.

Cassiani, G., Bruno, V., Villa, A., Fusi, N. & Binley, A.M., 2006. A saline tracer test monitored via time-lapse surface electrical resistivity tomography, *J. appl. Geophys.,* **59,** 244–259.

Chen, J., Hubbard, S.S., Williams, K.H., Pride, S., Li, L. & Slater, L., 2009. A state-space Bayesian framework for estimating biogeochemical transformations using time-lapse geophysical data, *Water Resour. Res.,* **45,** W08420, doi:10.1029/2008WR007698.

Cirpka, O.A. & Kitanidis, P.K., 2000. Characterization of mixing and dilution in heterogeneous aquifers by means of local temporal moments, *Water Resour. Res.,* **36,** 1221–1236.

Coleman, T.F. & Li, Y., 1996. An interior, trust region approach for nonlinear minimization subject to bounds, *SIAM J. Optim.,* **6,** 418–445.

Day-Lewis, F.D. & Lane, J.W., Jr., 2004. Assessing the resolution-dependent utility of tomograms for geostatistics, *Geophys. Res. Lett.,* **31,** L07503, doi:10.1029/2004GL019617.

Day-Lewis, F.D., Harris, J.M. & Gorelick, S.M., 2002. Time-lapse inversion of crosswell radar data, *Geophysics,* **67,** 1740–1752.

Day-Lewis, F.D., Lane, J.W., Jr., Harris, J.M. & Gorelick, S.M., 2003. Time-lapse imaging of saline-tracer transport in fractured rock using difference-attenuation tomography, *Water Resour. Res.,* **39**(10), 1290, doi:10.1029/2002WR0011722.

Day-Lewis, F.D., Singha, K. & Binley, A.M., 2005. Applying petrophysical models to radar traveltime and electrical-resistivity tomograms: resolution-dependent limitations, *J. geophys. Res.,* **110,** B08206, doi:10.1029/2004JB003569.

Day-Lewis, F.D., Lane, J.W., Jr. & Gorelick, S.M., 2006. Combined interpretation of radar, hydraulic and tracer data from a fractured-rock aquifer near Mirror Lake, New Hampshire, USA, *Hydrogeol. J.,* **14,** 1–14.

Day-Lewis, F.D., Chen, Y. & Singha, K., 2007. Moment inference from tomograms, *Geophys. Res. Lett.,* **34, 6**, L22404, doi:10.1029/2007GL031621

Deiana, R., Cassiani, G., Villa, A., Bagliani, A. & Bruno, V., 2008. Calibration of a vadose zone model using water injection monitored by GPR and electrical resistance tomography, *Vadose Zone J.,* **7,** 215–226.

Dorn, O., Miller, E.L. & Rappaport, C.M., 2000. A shape reconstruction method for electromagnetic tomography using adjoint fields and level sets, *Inverse Probl.,* **16,** 1119–1156.

Ernst, J.R., Maurer, H.R., Green, A.G. & Holliger, K., 2007. Full-waveform inversion of crosshole georadar data based on 2-D finite-difference time-domain solutions of Maxwell's equations, *IEEE Trans. Geosci. Remote Sens.,* **45**, 2807–2828.

Freyberg, D.L., 1986. A natural gradient experiment on solute transport in a sand aquifer. 2. Spatial moments and the advection and dispersion of nonreactive tracers, *Water Resour. Res.,* **22,** 2031–2046.

Friedel, S., 2003. Resolution, stability, and efficiency of resistivity tomography estimated from a generalized inverse approach, *Geophys. J. Int.,* **153,** 305–316.

Goltz, M.N. & Roberts, P.V., 1987. Using the method of moments to analyze three-dimensional diffusion-limited solute transport from temporal and spatial perspectives, *Water Resour. Res.,* **23,** 1575–1585.

Gorelick, S.M., Liu, G. & Zheng, C., 2005. Quantifying mass transfer in permeable media containing conductive dendritic networks, *Geophys. Res. Lett.,* **32,** L18402, doi:10.1029/2005GL023512.

Grisak, G.E., Pickens, J.F. & Cherry, J.A., 1980. Solute transport through fractured media. 2. Column study of fractured till, *Water Resour. Res.,* **16,** 731–739.

Guyod, H., 1944. Fundamental data for the interpretation of electric logs, *The Oil Weekly,* **115**(38), 21–27

Harbaugh, A.W., Banta, E.R., Hill, M.C. & McDonald, M.G., 2000. MODFLOW-2000, the U.S. Geological Survey modular ground-water model—User guide to modularization concepts and the Ground-Water Flow Process, U.S. Geological Survey Open-File Report 00–92, 121 pp.

Harvey, C. & Gorelick, S.M., 2000. Rate-limited mass transfer or macrodispersion: which dominates plume evolution at the Macrodispersion Experiment (MADE) site? *Water Resour. Res.,* **36,** 637–650.

Henderson, R.D., Day-Lewis, F.D., Harvey, C.F., Abarca, E., Karam, H.N., Liu, L. & Lane, J.W., Jr., 2010. Marine electrical resistivity imaging of submarine ground-water discharge: sensitivity analysis and application in Waquoit Bay, Massachusetts, USA, *Hydrogeol. J.,* **18,** 173–185, doi:10.1007/s10040-009-0498-z.

Hubbard, S.S., Williams, K., Conrad, M., Faybishenko, B., Peterson, J., Chen, J., Long, P. & Hazen, T., 2008. Geophysical monitoring of hydrological and biogeochemical transformations associated with Cr(VI) biostimulation, *Environ. Sci. Technol.,* **42**(10), 3757–3765, doi:10.1021/es071702s.

Johnson, T.C., Routh, P.S. & Knoll, M.D., 2005. Fresnel volume georadar attenuation difference tomography, *Geophys. J. Int.,* **162,** 9–24.

Johnson, T.C., Routh, P.S. & Knoll, M.D., 2007. A field comparison of Fresnel zone and ray-based GPR attenuation-difference tomography for time-lapse imaging of electrically anomalous tracer or contaminant plumes, *Geophysics,* **72,** G21–G29.

Johnson, T.C., Versteeg, R.J., Ward, A., Day-Lewis, F.D. & Revil, A., 2010. Improved hydrogeophysical characterization and monitoring through parallel modeling and inversion of time-domain resistivity and induced polarization data, *Geophysics,* **75**(4), 27–41, doi:10.1190/1.3475513.

Kemna, A., Vanderborght, J., Kulessa, B. & Vereecken, H., 2002. Imaging and characterisation of subsurface solute transport using electrical resistivity tomography (ERT) and equivalent transport models, *J. Hydrol.,* **267,** 125–146.

Kemna, A., Binley, A.M., Day-Lewis, F.D., Englert, A., Tezkan, B., Vanderborght, J. & Vereecken, H., 2006. Solute and contaminant transport monitoring, in *Applied Hydrogeophysics,* NATO Science Series IV: Earth and Environmental Sciences, Vol. 71, pp. 117–159, ed. Vereecken, H., Springer, Amsterdam, doi:10.1007/978-1-4020-4912-5_1.

LaBolle, E.M. & Fogg, G.E., 2001. Role of molecular diffusion in contaminant migration and recovery in an alluvial aquifer system, *Transport Porous Media,* **42,** 155–179.

Lane, J.W., Jr., Day-Lewis, F.D., Versteeg, R.J. & Casey, C.C., 2004. Object-based inversion of crosswell radar tomography data to monitor vegetable oil injection experiments, *J. Environ. Eng. Geophys.,* **9,** 63–77.

Lane, J.W., Jr., Day-Lewis, F.D. & Casey, C.C., 2006. Geophysical monitoring of field-scale vegetable oil injections for biostimulation, *Ground Water,* **44**(3), 430–443, doi: 10.1111/j.1745-6584.2005.00134.x.

Looms, M.C., Binley, A., Jensen, K.H., Nielsen, L. & Hansen, T.M., 2008a. Identifying unsaturated hydraulic parameters using an integrated data fusion approach on cross-borehole geophysical data, *Vadose Zone J.,* **7,** 238–248.

Looms, M.C., Jensen, K.H., Binley, A. & Nielsen, L., 2008b. Monitoring unsaturated flow and transport using cross-borehole geophysical methods, *Vadose Zone J.,* **8,** 227–237.

Meigs, L.C. & Beauheim, R.L., 2001. Tracer tests in fractured dolomite. 1. Experimental design and observed tracer recoveries, *Water Resour. Res.,* **37,** 1113–1128.

Menke, W., 1984. *Geophysical Data Analysis: Discrete Inverse Theory,* p. 289, Academic Press, London.

Michelena, R.J. & Harris, J.M., 1991. Tomographic traveltime inversion using natural pixels, *Geophysics,* **56,** 635–644.

Milanfar, P., Karl, W.C. & Willsky, A.S., 1996. A moment-based variational approach to tomographic reconstruction, *IEEE Trans. Image Process.,* **5,** 459–470.

Miller, E.L., Kilmer, M. & Rappaport, C., 2000. A new shape-based method for object localization and characterization from scattered field data, *IEEE Trans. Geosci. Remote Sens.,* **38,** 1682–1696.

Nguyen, F., Kemna, A., Antonsson, A., Engesgaard, P. & Ogilvy, R., 2009. Characterization of seawater intrusions using 2D electrical tomography, *Near Surf. Geophys.,* doi:10.3997/1873-0604. 2009025.

Nimmo, J.R., Perkins, K.S., Schmidt, K.M., Stock, J.D., Miller, D.M. & Singha, K., 2009. Hydrologic characterization of desert soils with varying degrees of pedogenesis. I. Field experiments evaluating plant-relevant soil-water behavior, *Vadose Zone J.,* **8,** 480–495 doi:10.2136/vzj2008.0052.

Sheng, J. & Schuster, G.T., 2003. Finite-frequency resolution limits of wave path traveltime tomography for smoothly varying velocity models, *Geophys. J. Int.,* **152,** 669–676.

Singha, K. & Gorelick, S.M., 2005. Saline tracer visualized with electrical resistivity tomography: field scale moment analysis, *Water Resour. Res.,* **41,** W05023, doi:10.1029/2004WR003460.

Singha, K. & Gorelick, S.M., 2006. Effects of spatially variable resolution on field-scale estimates of tracer concentration from electrical inversions using Archie's law, *Geophysics,* **71,** G83–G91.

Singha, K., Day-Lewis, F.D. & Lane, J.W., Jr., 2007. Geoelectrical evidence for bicontinuum transport in groundwater, *Geophys. Res. Lett.,* **34,** L12401, doi:10.1029/2007GL030019.

Slater, L., Zaidman, M.D., Binley, A.M. & West, L.J., 1997. Electrical imaging of saline tracer migration for the investigation of unsaturated zone transport mechanisms, *Hydrol. Earth Syst. Sci.,* **1,** 291–302.

Slater, L., Binley, A.M., Daily, W. & Johnson, R., 2000. Cross-hole electrical imaging of a controlled saline tracer injection, *J. appl. Geophys.,* **44,** 85–102.

Swarzenski, P.W. *et al*., 2006. Combined time-series resistivity and geochemical tracer to examine submarine groundwater discharge at Dor Beach, Israel, *Geophys. Res. Lett.,* **33**, doi:10.1029/2006GL028282.

Swarzenski, P.W., Simonds, F.W., Paulson, A.J., Kruse, S. & Reich, C., 2007. Geochemical and geophysical examination of submarine groundwater discharge and associated nutrient loading estimates into Lynch Cove, Hood Canal, WA, *Environ. Sci. Technol.,* **41,** 7022–7029.

Tikhonov, A.N. & Arsenin, V.Y., 1977. *Solutions of Ill-Posed Problems,* John Wiley & Sons, New York, NY.

Vanderborght, J., Kemna, A., Hardelauf, H. & Vereecken, H., 2005. Potential of electrical resistivity tomography to infer aquifer transport characteristics from tracer studies: a synthetic case study, *Water Resour. Res.,* **41,** W06013, doi:10.1029/2004WR003774.

Williams, K.H., Ntarlagiannis, D., Slater, L.D., Dohnalkova, A., Hubbard, S.S. & Banfield, J.F., 2005. Geophysical imaging of stimulated microbial biomineralization, *Environ. Sci. Technol.,* **39,** 7592–7600.

Williams, K.H. *et al*., 2009. Geophysical monitoring of microbial activity during stimulated subsurface bioremediation, *Environ. Sci. Technol.,* doi:10.1021/es900855j.

Zheng, C. & Wang, P.P., 1999. MT3DMS: a modular three-dimensional multispecies model for simulation of advection, dispersion and chemical reactions of contaminants in groundwater systems: documentation and user's guide, Contract Report SERDP-99–1. U.S. Army Engineer Research and Development Center, Vicksburg, MS, 202 pp.